

# Compact fiber tip modal interferometer for high-temperature and transverse load measurements

Chao Chen,<sup>1</sup> Yong-Sen Yu,<sup>1,3</sup> Xuan-Yu Zhang,<sup>1</sup> Rui Yang,<sup>1</sup> Cong-Cong Zhu,<sup>1</sup> Chuang Wang,<sup>1</sup>  
Yang Xue,<sup>1</sup> Feng Zhu,<sup>1</sup> Qi-Dai Chen,<sup>1,4</sup> and Hong-Bo Sun<sup>1,2</sup>

<sup>1</sup>State Key Laboratory on Integrated Optoelectronics, College of Electronic Science and Engineering, Jilin University, 2699 Qianjin Street, Changchun 130012, China

<sup>2</sup>College of Physics, Jilin University, 119 Jiefang Road, Changchun 130023, China

<sup>3</sup>e-mail: yuys@jlu.edu.cn

<sup>4</sup>e-mail: chenqd@jlu.edu.cn

Received April 26, 2013; revised July 4, 2013; accepted July 16, 2013;  
posted July 25, 2013 (Doc. ID 189588); published August 19, 2013

A compact fiber tip modal interferometer (FTMI) based on two-wave interference has been demonstrated. Its fabrication process is very simple, just involving fiber tapering by a fusion splicer. The effective sensing area of the FTMI has a small length of  $\sim 310$   $\mu\text{m}$ . The interference spectra of the fiber tips with different size and profile have been analyzed. The FTMI has a good mechanical strength and high-temperature stability. It can be used for high-temperature and transverse load sensing simultaneously in a harsh environment when two different attenuation peaks are chosen to be monitored. © 2013 Optical Society of America

OCIS codes: (060.2370) Fiber optics sensors; (120.0120) Instrumentation, measurement, and metrology; (280.4788) Optical sensing and sensors; (280.6780) Temperature.

<http://dx.doi.org/10.1364/OL.38.003202>

For decades, fiber-optic sensors have been extensively studied and applied in physical, chemical, and biomedical sensing fields due to their advantages of light weight, corrosion resistant, anti-electromagnetic interference, and remote sensing [1–12]. In practical applications, especially in harsh environments, how to realize the transverse load/pressure measurement at high temperature, and how to solve the problem of temperature cross sensitivity have been attracting much attention. In previous reports, fiber Bragg grating (FBG) with load-induced birefringence [1] and long period fiber grating with orientation-dependent resonant dips [2] have been used for detection of the temperature and transverse load simultaneously. In order to realize the thermal strength of the grating structure, the femtosecond laser written [3,4] or thermally regenerated FBGs [5] are needed. In addition, the high-temperature pressure sensor based on high birefringence fiber, and microstructured optical fiber [6–9] modal interferometers are also proposed. However, these kinds of fiber sensors have complicated fabrication processes, high cost, and complex structures, limiting their mass production and practical application. Moreover, their feature sizes are at least several millimeters, making the measurement in small area and fixed point sensing difficult. So how to simplify the preparation technology and fabricate a simple-structured, compact, and low-cost fiber-optic sensor is always the aim to pursue [10].

In this Letter, we demonstrate a compact fiber tip modal interferometer (FTMI) sensor based on two single-mode fibers (SMFs) fusion at the end. The two SMFs are parallelly put in a fusion splicer, which is set to the tapering mode. The FTMI is formed when the two SMFs are fused and tapered to break. This sensor structure is high-temperature stable. Its operation temperature can be as high as  $1000^\circ\text{C}$ . Based on the special

fiber tip structure, transverse load measurement is realized. In addition, we carry out the simultaneous sensing of transverse load and high temperature via two different resonant dips, which have different responses to these environmental parameters.

The fabrication process and measurement setup for the FTMI are shown in Fig. 1(a). Two SMFs (SMF-28e, Corning) are connected with a supercontinuum broadband source (BBS) and an optical spectrum analyzer

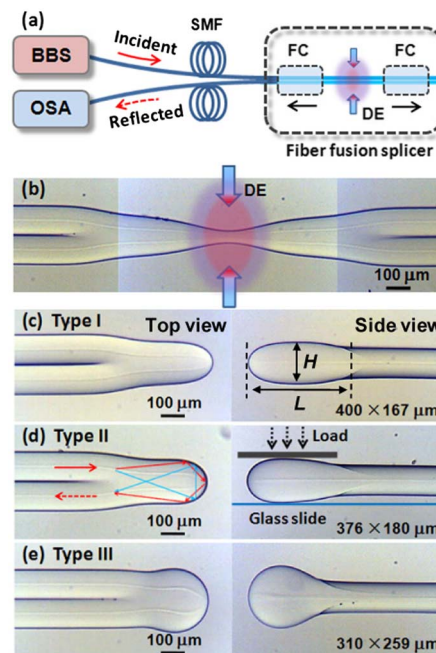


Fig. 1. (a) Fabrication and measurement setup for the FTMI. (b) Fiber-coupler-like structure formed by the tapering process with a fusion splicer. (c)–(e) Top and side views of the FTMIs fabricated with different discharge time.

(OSA, AQ6370B, Yokogawa), respectively, to monitor the interference spectrum. The fabrication process, similar to manufacturing a fiber coupler, is implemented in a fusion splicer (Ericsson FSU-975). First, the two fibers with coating removed were parallelly fixed in the fiber clamps (FCs) and under the discharge electrodes (DEs). Then the fibers were tapered and fused together, forming a fiber-coupler-like structure, as shown in Fig. 1(b). Finally, the coupler-like structure was tapered to break and generated two rounded-end fiber tips with similar profile and reflection spectrum. The size and morphology of the fiber tips can be controlled by adjusting the discharge current and time. When the discharge current was set as 18 mA and discharge time were 15.5, 16.0, and 17.0 s, respectively, three FTMI with different morphology were fabricated. Their top and side views are shown in Figs. 1(c)–1(e) and the corresponding sizes are  $L \times H = \sim 400 \times 167 \mu\text{m}$ ,  $\sim 376 \times 180 \mu\text{m}$ ,  $\sim 310 \times 259 \mu\text{m}$ , which are almost a tenth of the reported micro-fiber coupler tip in [11]. And the mechanical strength is significantly improved.

The operation principle of the FTMI can be described as follows. When light propagates from the incident fiber to the fiber tip, cladding modes are excited at the abrupt shoulder first. Later, the light propagates to the end of the device and is reflected by the spherical surface of the end, stimulating higher-order cladding modes. Then, some of the cladding modes couple back into the core mode of the output fiber. The phase difference between core and cladding modes accumulated via multiple reflections in the fiber tip will induce the mode interference. The interference spectra of the three configurations (Fig. 1) are shown in Fig. 2. The solid and dashed lines are the reflection spectra of the two FTMI from the two sides of one broken-off taper. The differences between the two sets of spectra may derive from asymmetry of the two DEs and minor different moving speed of the two motors. The sine-like spectrum implies that the FTMI may work in the form of two-wave interference. The interference spectra in Fig. 2 can be analyzed by fast Fourier transform and the corresponding spatial frequency spectra are obtained in Fig. 3. According to the spatial frequency equation  $\xi \approx \Delta n_{\text{eff}} L_{\text{eff}} / \lambda^2$ , assuming  $\lambda = 1550 \text{ nm}$  and  $\Delta n_{\text{eff}} =$

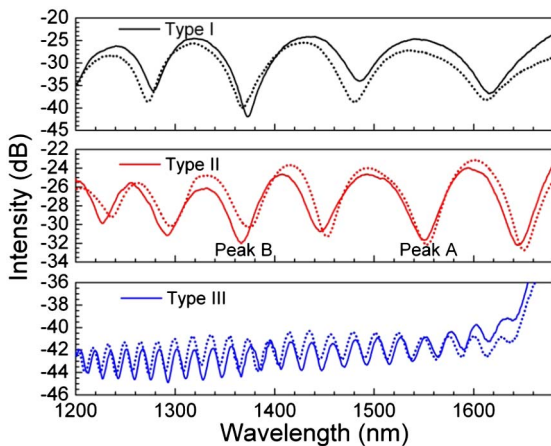


Fig. 2. Interference spectra corresponding to the FTMI in Figs. 1(c)–1(e).

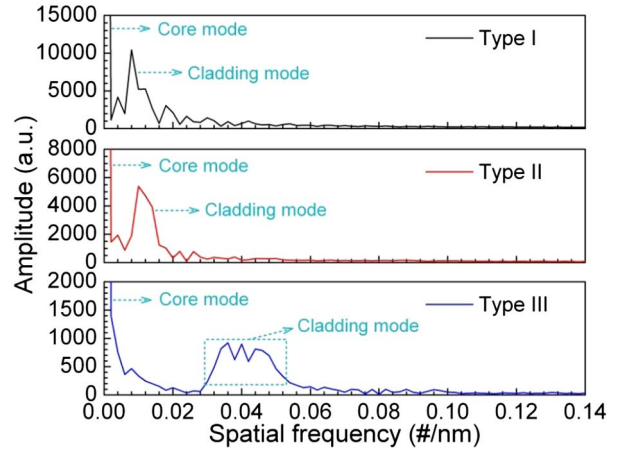


Fig. 3. Spatial frequency spectra corresponding to the FTMI in Figs. 1(c)–1(e).

0.025, the effective physical lengths  $L_{\text{eff}}$  are calculated to  $\sim 769$ ,  $\sim 961$ , and  $\sim 3844 \mu\text{m}$ , respectively [7]. Apparently,  $L_{\text{eff}} > L$ , indicating light experiences multireflection in the fiber tip. With the device size decreasing, its reflection time increases to generate a long optical path difference (OPD,  $\Delta n_{\text{eff}} L_{\text{eff}}$ ). That is why the  $\xi$  of FTMI increases with its actual size decreasing. It should be noted that, multiple reflection will increase the transmission loss and depress the extinction ratio of the interference fringe (Fig. 2).

To research the FTMI's transverse load and high-temperature sensing characteristics, we take the device corresponding to Fig. 1(d) for example to analyze. We chose the attenuation peaks A and B in the reflection spectrum and monitored their change with the variation of environmental perturbations. In the transverse load measurement, the FTMI was horizontally placed between two parallel glass slides, as shown in Fig. 1(d). With loads increasing, the spectrum had a blueshift, as shown in Fig. 4(a). This may be caused by the OPD between interference modes decreasing with the transverse load augment. The transverse load sensitivities of peaks A and B were determined to be  $-252.6 \text{ pm/N}$  and  $-173.6 \text{ pm/N}$  by linear fitting the experimental results. As for the high-temperature test, the FTMI was positioned in a tube furnace with temperature from room temperature ( $20^\circ\text{C}$ ) to  $1000^\circ\text{C}$ . Here, thermal-optic and thermal-expansion effects induced the redshift of interference spectrum. Figure 4(b) shows the linear relationships between attenuation peaks A and B with temperature, and their temperature sensitivities are  $14.6 \text{ pm}/^\circ\text{C}$  and  $12.5 \text{ pm}/^\circ\text{C}$ , respectively, which are similar with that of the FBG [3].

In order to discriminate the transverse load and temperature, the sensitivity matrix is applied. The wavelength change ( $\Delta\lambda_A, \Delta\lambda_B$ ) of peaks A and B as functions of transverse load and temperature ( $\Delta N, \Delta T$ ) can be expressed as

$$\begin{pmatrix} \Delta\lambda_A \\ \Delta\lambda_B \end{pmatrix} = \begin{pmatrix} k_{A,N} & k_{A,T} \\ k_{B,N} & k_{B,T} \end{pmatrix} \begin{pmatrix} \Delta N \\ \Delta T \end{pmatrix} = K \begin{pmatrix} \Delta N \\ \Delta T \end{pmatrix}, \quad (1)$$

where  $k_{A,N}$  and  $k_{B,N}$  are the transverse load sensitivities of the peaks A and B, respectively,  $k_{A,T}$  and  $k_{B,T}$  are their

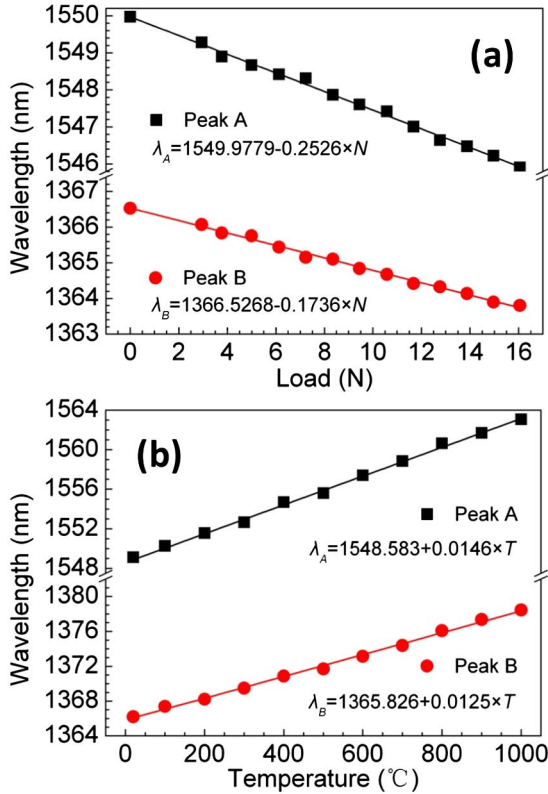


Fig. 4. Responses of (a) transverse load and (b) temperature of the peaks A and B for the FTMI in Fig. 1(d).

temperature sensitivities. The measurement resolutions of the transverse load and temperature are expressed as

$$\begin{pmatrix} \delta(\Delta N) \\ \delta(\Delta T) \end{pmatrix} = \pm \frac{1}{|D|} \begin{pmatrix} |k_{B,T}| & |k_{A,T}| \\ |k_{B,N}| & |k_{A,N}| \end{pmatrix} \begin{pmatrix} |\delta(\Delta \lambda_A)| \\ |\delta(\Delta \lambda_B)| \end{pmatrix}, \quad (2)$$

where  $D$  is the determinant value of the matrix. A relatively large  $D$  is desirable to improve the sensing resolution. The resonant dips wavelength resolutions ( $\delta(\Delta \lambda_A)$ ,  $\delta(\Delta \lambda_B)$ ) are dependent on the noise of the measuring instrument and also on the dips shape [12]. Here we choose the OSA resolution of 20 pm to simplify the analysis. We substitute the sensitivities obtained from experiments to the matrix above and get the condition number  $\text{cond}(K) = 151.39$ , which is related to the matrix stability [13]. The relatively large number may increase the measurement errors. Fortunately, the determinant value of the matrix ( $D = -622.94$ ) is also large and can effectively improve the measurement resolutions. According to Eq. (2),

the measurement resolutions of the transverse load and temperature are calculated to  $\pm 0.87N$  and  $\pm 1.37^\circ C$ , respectively. It should be noted that the calculated results are less than the true values due to the simplification.

In conclusion, we have fabricated a compact fiber tip interferometer just by using a fusion splicer, making the fabrication process simple and low cost. The effective sensing area of the fiber tip is only about 310  $\mu m$ . The reflection spectrum of the FTMI is dependent on the size and profile of the fiber tip. The simple-structured fiber sensor not only has a similar temperature sensitivity with the FBG fabricated via the complicated method, but also has an excellent high-temperature stability and mechanical strength. It can be used for simultaneous sensing of transverse load and temperature in harsh environments even in temperatures up to 1000°C. In addition, due to the small size and operation at the reflection mode, the FTMI has potential applications for localized area/fixed point and remote sensing.

This work was supported by the National Natural Science Foundation of China under grants 90923037, 91123027, and 61137001.

## References

1. H. Chi, X. M. Tao, D. X. Yang, and K. S. Chen, *Opt. Lett.* **26**, 1949 (2001).
2. Y. J. Rao, Y. P. Wang, Z. L. Ran, and T. Zhu, *J. Lightwave Technol.* **21**, 1320 (2003).
3. C. Chen, Y. S. Yu, R. Yang, L. Wang, J. C. Guo, Q. D. Chen, and H. B. Sun, *J. Lightwave Technol.* **29**, 2126 (2011).
4. C. M. Jewart, Q. Wang, J. Canning, D. Grobnc, S. J. Mihailov, and K. P. Chen, *Opt. Lett.* **35**, 1443 (2010).
5. H. M. Kim, T. H. Kim, B. Kim, and Y. Chung, *Appl. Opt.* **49**, 3841 (2010).
6. T. Chen, Q. Wang, R. Chen, B. Zhang, C. Jewart, K. P. Chen, M. Maklad, and P. R. Swinehart, *Opt. Lett.* **37**, 1064 (2012).
7. C. Wu, H. Y. Fu, K. K. Qureshi, B. O. Guan, and H. Y. Tam, *Opt. Lett.* **36**, 412 (2011).
8. J. Ma, J. Ju, L. Jin, W. Jin, and D. Wang, *Opt. Express* **19**, 12418 (2011).
9. J. Limpert, F. Stutzki, F. Jansen, H. J. Otto, T. Eidam, C. Jauregui, and A. Tunnermann, *Light Sci. Appl.* **1**, 1 (2012).
10. R. Yang, Y. S. Yu, Y. Xue, C. Chen, Q. D. Chen, and H. B. Sun, *Opt. Lett.* **36**, 4482 (2011).
11. M. Ding, P. F. Wang, and G. Brambilla, *Opt. Express* **20**, 5402 (2012).
12. H. P. Looocka and P. D. Wentzell, *Sens. Actuators B* **173**, 157 (2012).
13. A. M. Vengsarkar, W. C. Michie, L. Jankovic, B. Culshaw, and R. O. Claus, *J. Lightwave Technol.* **12**, 170 (1994).